Volume 1 | Number 1 | Jan 2013 | Pages 1–100

Journal of
Materials Chemistry A

Materials for energy and sustainability
www.rsc.org/materialsA

ROYAL SOCIETY
OF CHEMISTRY

ROYAL SOCIETY
OF CHEMISTRY

www.rsc.org/materialsA

Journal Name

ARTICLE TYPE

Well-defined carbon polyhedrons prepared from nano metal-organic frameworks for oxygen reduction

Wei Xia, Jinghan Zhu, Wenhan Guo, Li An, Dingguo Xia and Ruqiang Zou*

We report a nanostructured electrocatalyst engineered from molecular design and morphology evolution. A typical Co-based metal-organic frameworks, ZIF-67 nanocrystals were precisely synthesized with tunable size and morphology. Nitrogen doped carbon nano polyhedrons decorated with cobalt nanoparticles were fabricated via pyrolysis of ZIF-67 and the carbonized products inherited the nano-size

10 and shape of the MOF precursor. The intense effect of size on the electrocatalytic activity and transport properties was systematically investigated. Catalyst derived from the smallest MOF (300nm), exhibited superior performance towards oxygen reduction with an onset potential of 0.86 V and half-wave potential of 0.71 V in acidic solution, which are comparable to the best carbon-based ORR catalysts. This work will pave the way for the development of MOF-derived energy materials in various fields such as fuel

15 cells and Li-air batteries, and opens new avenues for the design of MOFs in electrochemical application.

Introduction

Developing highly efficient electrocatalysts for oxygen reduction reaction (ORR) has long been a hot topic in developing fuel cells and Li-air batteries.[1,2] To date, Pt and its alloys are still the most

20 efficient catalyst.[3,4] However, due to the high cost and scarcity, large-scale application of platinum based catalysts is prohibited.[5] As alternatives, nanostructured carbon-based materials have emerged and attracted great attention.[6,7] For example, N- and O-doped mesoporous carbons,[8] nitrogen-doped nanotubes arrays,[9]

25 Co$_3$O$_4$/N-doped graphene hybrid[10] and carbon nanotube-graphene complexes,[11] have been reported to offer good ORR activities and some are almost comparable to platinum based catalysts in alkaline media. However, in acidic environment, the performance and especially the stability of most of the carbon-based catalysts

30 is poor. Addition of some metal species into the nitrogen doped carbons was found to improve the activity. Wu et al. reported polyaniline derived catalyst incorporating iron and cobalt,[12] which showed small ORR overpotential and good stability. Lefèvre et al. prepared microporous carbon-supported Fe-based

35 catalysts with improved ORR activity.[13] Although there are still some performance gap between those catalysts and Pt/C, these works revealed new prospect to achieve highly active non-precious ORR catalysts by increasing the active sites on surface. It is profitable to prepare nanostructured catalyst from

40 morphology evolution and molecular design.

On the other side, metal-organic frameworks (MOFs), built from the coordination of metal ions and organic ligands, possess defined and tunable structures at a molecular level. Owing to their properties unique like high surface areas, tunable pore sizes

45 and multi functionalities,[14-16] MOFs have been widely studied and utilized in areas such as gas storage/separation,[17] catalysis,[18]

magnetic material,[19] and luminescence.[20] Recently, MOFs were used as novel self-sacrificed templates to prepare nanostructured materials like porous carbons and metal oxides.[21-30] This strategy

50 is fascinating because carbons or metal oxides with extremely porous structures can be obtained directly from MOFs without extra templates. These MOFs derived materials are promising candidates in hydrogen storage,[22,23] sensor,[24] electrochemical capacitor[26] and lithium ion battery.[27-29] However, only a few

55 works on MOF derived materials for ORR catalysis have just been published.[31-34] MOFs with high contents of nitrogen like Co-ZIF, Fe-ZIF and ZIF-8 were applied in this investigation. Moreover, to the best of our knowledge, the reported works were based on the selection of due type of MOF. There was no

60 investigation about the size effect of MOFs on the catalytic performance.

In this study, we developed a new ORR electrocatalyst from metal-organic frameworks (MOFs). This is the first report of the MOF-derived nanomaterials with catalytic performance highly

65 dependent on the size of the MOF precursors. Uniform ZIF-67 precursors of various crystalline sizes ranging from 300 nm to several micrometers were well-controlled synthesized. Comparison between these MOF-derived catalysts leads us to the conclusion that the ORR activity and stability increases as the

70 size of the precursor decreases. Carbon polyhedrons prepared from the smallest nano-MOF exhibits the highest ORR activity with an onset potential of 0.86 V and a half-wave potential of 0.71 V, which are superior to those of the larger MOF derived catalysts and are among the highest values for non-precious

75 catalysts reported so far.

Experimental Section

Synthesis of ZIF-67 and ZIF-67 derived catalysts

Bulk ZIF-67: Bulk ZIF-67 was synthesized through the following solvothermal procedure: $Co(Ac)_2\cdot4H_2O$ (3.321 g, 40/3 mmol) and 2-methylimidazole (3.284 g, 40 mmol) were dissolved in 100 mL ethanol in a 125 mL Teflon-lined steel autoclave. The autoclave was sealed, heated up to 120 °C and kept at this temperature for 3 days. The as-made crystals were filtered out and washed by ethanol, finally dried under vacuum at 150 °C for 8 hours. The products were dark purple crystals.

1.7 μm ZIF-67: 0.450 g of $Co(NO_3)_2\cdot6H_2O$ was dissolved in 12 mL deionized water, and 5.500 g of 2-methylimidazole was dissolved in 80 mL deionized water. Then they were mixed under vigorous stirring at 60 °C. The mixture gradually turned to milky colloidal dispersion. After 12 minutes, stirring was stopped and the mixture was kept for 20 hours. After that, the dispersion was centrifuged and washed with methanol for three times. Then the product was vacuum dried at 150 °C for 8 hours.

800 nm ZIF-67: Typically, 1.436 g of $Co(NO_3)_2\cdot6H_2O$ and 3.244 g of 2-methylimidazole were each dissolved in 100 mL methanol at 60 °C. The former salt solution was poured into the latter ligand solution under vigorous stirring. The mixture was stirred for 12 minutes and kept for 20 hours. Solid product was separated by centrifugation and washed with methanol for three times, followed by vacuum drying at 150 °C for 8 hours.

300 nm ZIF-67: The procedure was similar to that described above for 800 nm ZIF-67, instead, the reaction temperature was reduced to 25 °C.

For the preparation of ZIF-67 derived carbons, the above prepared ZIF-67 precursors were pyrolyzed at temperatures ranged from 600-900 °C for 2 hours under an argon gas flow and cooled down to room temperature naturally.

Characterization

Powder X-ray diffraction patterns were collected on a Bruker D8 Advanced diffractometer at 40 KV and 40 mA and using Kα radiation (λ = 1.5406 Å). Thermogravimetric analyses (TGA) were carried out on a TA Instruments SDT Q600 analyzer under nitrogen flow. Scanning electron microscopy (SEM) images were recorded on a Hitachi S-4800. Transmission electron microscopy (TEM) images and selected area electron diffraction (SAED) were taken on a FEI Tecnai T20 microscope. X-ray photoelectron spectroscopy (XPS) measurements were performed on a Kratos Axis Ultra Imaging Photoelectron Spectrometer using monochromatic Al Kα line (1486.7 eV). Nitrogen sorption measurements at 77 K were carried out by a Quantachrome Autosorb-IQ gas adsorption analyzer. Before the sorption tests, samples were degassed at 250 °C for 8 h under dynamic vacuum. The resulting BET surface areas were calculated from the adsorption branches. Pore size distributions were fitted from Quenched Solid Density Functional Theory (QSDFT) based on the desorption branches.

Electrochemical measurements

For the preparation of working electrodes, 2 mg of catalyst was dispersed in 2 mL of ethanol under sonication for 1 h to form a homogeneous catalyst ink. Then 80 μL of this catalyst ink was loaded onto a glassy carbon rotating disk electrode (diameter 5 mm), resulting in the catalyst loading of 0.4 mg cm^{-2}. The electrode was dried under atmospheric condition, followed by dropping 5 μL of 0.1 wt% Nafion suspension in ethanol as a binder.

Cyclic voltammetry (CV) and rotating disk electrode (RDE) measurements were conducted on a CHI electrochemical workstation (Model 760C) with a standard three-electrode system. The catalyst coated glassy carbon electrode was used as the working electrode, an Ag/AgCl electrode in saturated KCl solution and Pt foil work as the reference and counter electrodes, respectively. All initially measured potentials were converted to a RHE scale. The electrolyte was 0.1 M perchloric acid ($HClO_4$). All electrochemical measurements were performed at room temperature.

Koutechy-Levich plots were analyzed at different potentials. The number of electrons transferred (n) during the oxygen reduction reaction (ORR) were calculated from the slopes of their linear fit lines based on the Koutechy-Levich equation:

$$\frac{1}{J} = \frac{1}{J_L} + \frac{1}{J_K} = \frac{1}{B\omega^{1/2}} + \frac{1}{J_K} \tag{1}$$

$$B = 0.62nFC_0(D_0)^{2/3}\nu^{-1/6} \tag{2}$$

$$J_K = nFkC_0 \tag{3}$$

Where J is the measured current density, J_L and J_K are the diffusion- and kinetic limiting current densities, ω is the rotation speed (rad s^{-1}), n is transferred electron number, F is the Faraday constant (96485 C mol^{-1}), C_0 is the O_2 concentration in the electrolyte (1.26 × 10^{-6} mol cm^{-3}), D_0 is the diffusion coefficient of O_2 in the electrolyte (1.93 × 10^{-5} cm^2 s^{-1}), and ν is the kinetic viscosity of 0.1 M perchloric acid (0.01009 cm^2 s^{-1}).

Results and Discussion

Our studies are based on nano zeolitic imidazolate frameworks (ZIFs), a subclass of MOFs that possess exceptional chemical/thermal stability and high surface area.[35,36] Specifically, ZIF-67 was chosen for the target investigation. In this MOF, each cobalt cation is bridged with four nitrogen atoms from the 2-methylimidazolate anions into tetrahedral frameworks and further assembles into a sodalite (SOD) topology. Although it is challenging to define the resolved structure of the ORR active sites in non-precious catalysts after so many works, M-N-C (M: Fe and/or Co) structure has been proved to be closely related to the ORR active site.[31] Given the abundant Co-N4 moieties and high surface area of ZIF-67, we expected to obtain a porous carbon with high content of Co-N and high surface area. Meanwhile, by reducing the size of the MOF precursor to nano size, we hoped to improve the mass and electron transfer efficiency from the derived nanoscale structured catalytic system.

In the preparation of size controlled nanoparticles, modulators such as polymers or surfactant are often used, which is also applicable in MOF synthesis.[37,38] However, in further applications, complete removal of those modulators is essential but hard to achieve. Other methods, such as microwave[39] and ultrasound[40] were also applied to produce small size MOFs, however, the process is still complicated and requiring high energy consumption. Here, by simply altering the solvent and reaction temperature, we achieved well-defined monodisperse ZIF-67 crystals with different sizes (Fig. 1). The smallest ZIF-67 crystals with an average particle size of 300 nm were synthesized at room temperature using methanol solvent (Fig. S1,S2). By

ARTICLE TYPE
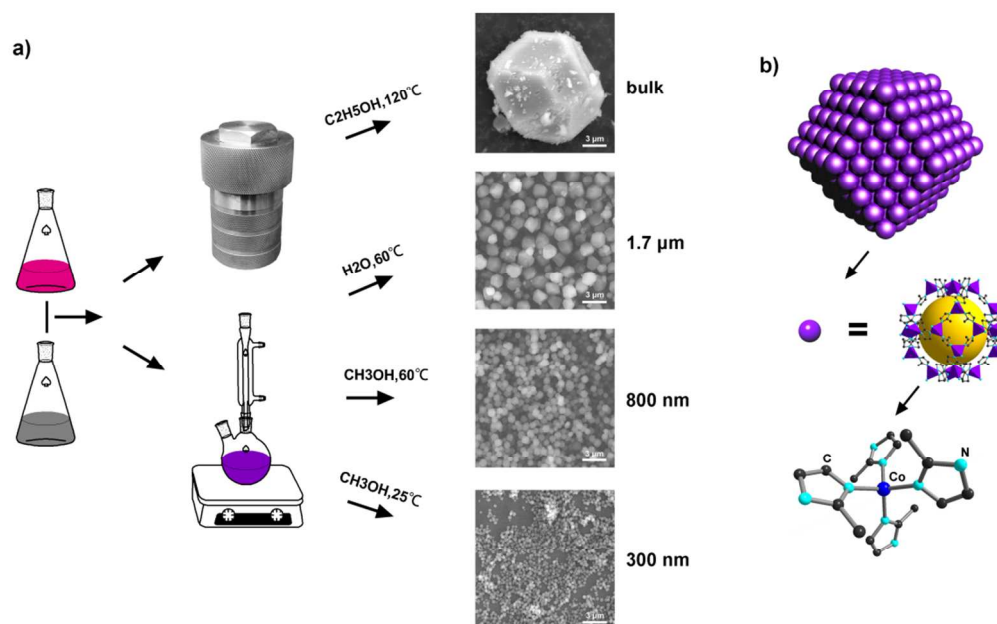
Fig.1 Synthesis of ZIF-67 with various sizes. (a) Schematic showing the synthetic procedures. (b) Structure information of the ZIF-67 crystal.

slightly elevating the reaction temperature to 60 °C to accelerate crystal growth, we obtained larger particle sizes of 800 nm (Fig.
5 S3,S4). The increase in particle size may result from further growth via aggregation of the initially formed nuclei at the higher temperature. Replacing methanol by more polar solvent like water, the particle size was further increased to an average size of 1.7 μm (Fig. S5,S6). For comparison, bulk ZIF-67 crystals were
10 synthesized through a solvothermal procedure. The resulting products have a wide size distribution from several micrometers to several hundred micrometers (Fig. S7). Powder X-ray diffraction (PXRD) shows that all products are ZIF-67 crystals without any detectable by-products (Fig. S8).

15 For the preparation of ORR catalyst, the above ZIF-67 nano- and microcrystals were subjected to heat treatment under argon atmosphere. The morphologies of samples after heat treatment were characterized by scanning electron microscopy (SEM) and transmission electron microscopy (TEM) (Fig. 2a-f and Fig. S9-
20 12). The rhombic dodecahedral shape of the MOF precursor is well preserved in the MOF derived catalyst (denoted as MDC). It can be seen that in the carbon polyhedrons, darker dots with the size of ~10 nm are well dispersed in the matrixes (Fig. 2f,g). These dots were further proved to be cobalt nanoparticles by
25 selected area electron diffraction (SAED) (Fig. 2h) and PXRD (Fig. 2i) analyses. Magnification of the cobalt nanoparticles shows that they are wrapped by a few layers carbon sheets (Fig. 2g), which are in-situ generated under the catalytic effect of cobalt metal at high temperature.

30 Nitrogen sorption experiments were conducted to investigate the pore textures of MDCs. Before heat treatment, the MOF precursor exhibits typical type-I isotherms (Fig. 3a) implying the microporous structure in the precursor. The Brunauer-Emmett – Teller (BET) surface area was found to be 1512 m^2 g^{-1}. After heat
35 treatment at 750 °C, the product displayed a bit similar isotherms to those of the precursor (Fig. 3a). The high uptake at low relative pressure suggests the dominating micropores in the sample. The slight hysteresis loops between the adsorption and desorption branches and vertical tails at around 1.0 relative pressure reveal
40 the presence of certain portion of meso- and macropores. Although the BET surface area decreases drastically after heat treatment, the resultant MDC keep a high surface area of 386 m^2 g^{-1}. The detail of the pore structure changes after heat treatment is displayed by the pore size distributions (PSD) (Fig. S13). The
45 ZIF precursor has a narrow PSD mainly focused on 0.9 nm. After heat treatment, mesopores with the ranges of 2.0 nm to 5.0 nm and pores larger than 26 nm were formed. For the MDC samples prepared from different sized MOFs, the surface areas were also examined by nitrogen sorption experiments (Fig. S14). As the
50 size increases, the BET surface area decreases. The value was found to be 326 m^2 g^{-1} for MDC from the 800 nm crystal, and 233 m^2 g^{-1} for 1.7 μm sample. The bulk sample has the lowest BET surface area of 165 m^2 g^{-1}. However, the corresponding pore size distributions are very similar (Fig. S15).

55 The oxygen reduction properties of the MDCs were evaluated by cyclic voltammetry (CV) and rotating disk electrode (RDE) measurements in 0.1 M HClO$_4$. Each material with the same mass was loaded onto a glassy carbon electrode (0.4 mg cm^{-2}). In CV tests, featureless voltammetric currents in the selected potential

ARTICLE TYPE
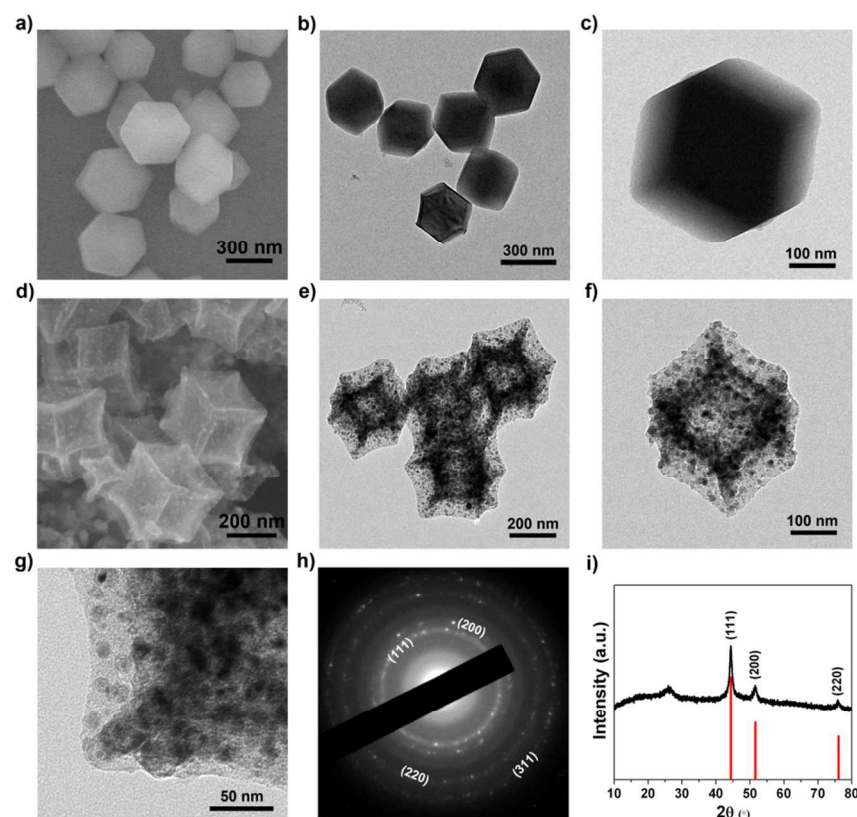
Fig. 2 (a) SEM image of the as-prepared 300 nm ZIF-67. (b,c) TEM images of the ZIF-67 at different magnifications. (d) SEM image of ZIF-67 after heat treatment at 750 °C. (e-g) TEM images of the 750 °C treated ZIF-67. (h,i) SAED (h) and XRD (i) patterns of the ZIF-67 treated at 750 °C.

ranges are obtained for all samples in Ar. In contrast, they
5 displayed well-defined cathodic peaks in O_2 (see Fig. 3b and Supplementary information). Insight of the ORR kinetics was revealed by RDE tests. Fig. 3c shows the RDE polarization curves at different potential for 300 nm MDC prepared at 750 °C. The ORR onset and half-wave potential are as high as 0.86 V and
10 0.71 V relative to the reversible hydrogen electrode (RHE). These rank the 300 nm MDC among the best non-precious ORR catalysts reported so far (see Table S1).[41] The corresponding Koutecky-Levich plots exhibits good linearity and near parallelism at various potentials (Fig. 3d), which suggested first-
15 order reaction kinetics to the dissolved oxygen concentration.

The effect of the size to the catalysis performance was studied. As shown in Fig. 4a, the RDE polarization plots at 1600 rpm were recorded for all MDC samples. As the size of the precursor decrease, the derived catalysts show increased ORR catalytic
20 activity. Catalyst prepared from bulk ZIF-67 crystal showed some ORR activity with an onset potential of 0.80 V, and very limited kinetic current density J_k. As the size decreases, the onset potential and kinetic current density increase. The smallest MDC (300 nm) exhibited markedly higher ORR than those of the larger
25 MDCs, with a much higher ORR onset potential and well-defined plateau representing diffusion-limiting currents in the RDE

polarization plots. Remarkably, the kinetic current densities J_k for 300 nm MDC are significantly higher than the larger samples at the same loading (Fig. 4c). Currents normalized to the weight are
30 showed in Fig. S24.

The electron transfer number (n) for the different samples provides a direct evidence of the size effect on catalyst performance. Fig. 4b compares the electron transfer number for the MDC with various sizes at different potentials. In ORR
35 system, oxygen can be reduced via two pathways, four- and two-electron transfer processes, in which four-electron transfer process is preferred.[42] Here, 300 nm MDC gave the highest and nearly stable electron transfer number with an average value of 3.7 in the potential range of 0-0.7 V, implying a dominative four-
40 electron pathway. When the size comes to a larger 800 nm, the corresponding catalyst gave decreased electron transfer numbers with an average value of 3.5 in the potential range. Further increasing the particle size to 1.7 μm leads to a lower n value of 3.2. As expected, bulk crystal derived catalyst gave the lowest n
45 value of 2.8. Notice that the high amount of loaded catalyst on the electrode will influence of the detection of the produced peroxide and thus the higher n value.[43] Test of the 300 nm sample with a low loading of 0.1 mg cm^{-2} was performed under the same condition (Fig. S25). It also exhibits high electron transfer

Journal Name

ARTICLE TYPE
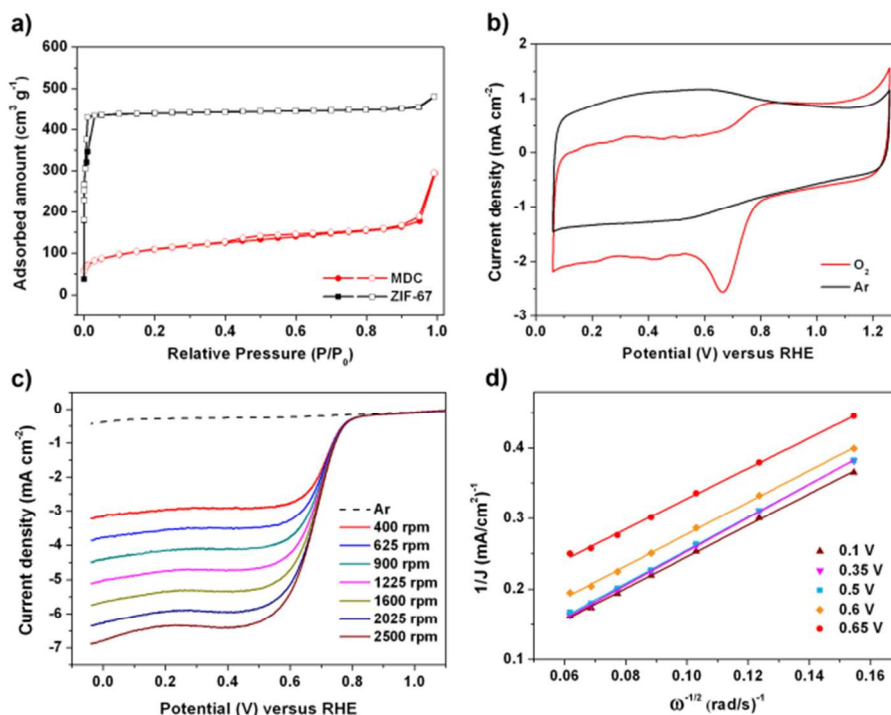
Fig. 3 Gas sorption and ORR performances of 300 nm MDC prepared at 750 °C. (a) Nitrogen sorption isotherms at 77 K of 300 nm ZIF-67 and its derived catalyst. (b) CV curves in O_2 saturated (red line) or Ar-saturated (black line) 0.1 M $HClO_4$ with a sweep rate of 50 mV s^{-1}. (c) RDE polarization curves in O_2 saturated (solid line) or Ar-saturated (dash line) 0.1 M $HClO_4$ at various rotation rates. (d) Koutecky-Levich plots at different potentials.
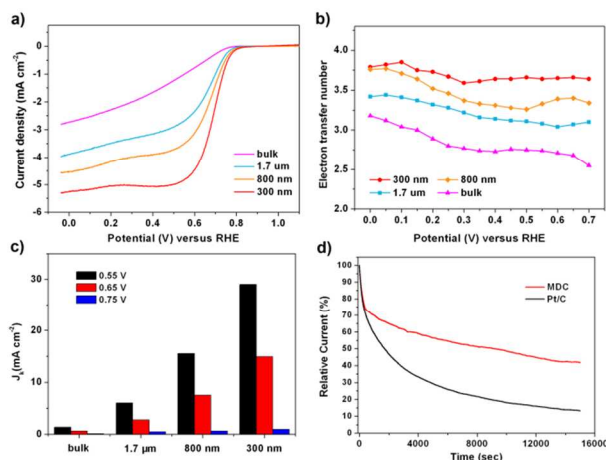
Fig. 4 (a) RDE polarization curves of 300 nm, 800 nm, 1.7 μm and bulk MDCs in 0.1 M $HClO_4$ at a rotation rate of 1600 rpm. (b) The electron transfer number as a function of potential for MDCs with various sizes. (c) Specific activities at various potentials for MDCs of different sizes. (d) Stability evaluation of Pt/C (black) and 300 nm MDC (red) in an O_2-saturated 0.1 M $HClO_4$ at 0.65 V and rotation speed of 1600 rpm.

numbers over the potentials. The superior ORR catalytic activity of the 300 nm MDC suggests that the smaller structure could provide more active and easily accessible catalytic centers and thus promote a faster mass and electron transfer process. This will be helpful for developing highly efficient catalysts from structure design in the future.

Particularly, M-N/C catalysts are known for the instability in acidic media and their practical application suffers from this limitation.[44] Surprisingly, MDC shows good stability. Tests were performed at 0.65 V in an O_2-saturated 0.1 M $HClO_4$ solution (Fig. 4 d). The commercial Pt/C catalyst shows a drastic current loss of approximately 87 % after 15000 seconds. However, MDC exhibited a very low attenuation after a 58 % loss indicating a superior stability than Pt/C in acid medium. It is interesting to find that the cobalt nanoparticles in our catalysts are stable in both acid medium and air. It is known that small sized metal particles like iron and cobalt are rather active and can burn in air. Here, the stability of the cobalt metal in the carbon matrix is due to the protection from the graphene-like carbon shells around the cobalt nanoparticles.

In catalyst preparation, the heat activation temperature is a key factor that directly affects the catalytic activity. Fig. 5a shows the results from RDE measurement of the MDC prepared at different temperature. The activity of the catalyst synthesized at 600 °C is very low in view of ORR onset and half-wave potentials. However, the activity increases as the heat treatment temperature rises, and comes to a peak at 750 °C. Then the activity drops down upon raising the temperature. The chemical surface

analysis by X-ray photoelectron spectroscopy (XPS) helped to reveal the changes over the temperatures. The full spectra of those samples show the presence of C, Co, N and O species (Fig. S34). The contents of each element were summarized in Table S2.
5 The results show that, as the pyrolysis temperature increased, the content of carbon in the catalyst increased while the nitrogen content declined drastically. That's because of the instability of nitrogen doped in carbons at elevated temperatures. A slight decrease in the content of the surface cobalt species was also
10 observed from the XPS result, which may result from the aggregation of cobalt species at high temperatures. Specially, nitrogen has been view as n-type carbon dopant, which can facilitate the ORR.[12] Thus nitrogen content and species in catalyst is critical in controlling the activity.[45] High-resolution N 1s XPS
15 spectra were collected to obtain insight into the nitrogen species in these catalysts (Fig. 5b-d). Results show subtle differences in the nitrogen species controlled by the heat activation temperature. The spectra can be deconvoluted into four peaks, which correspond to pyridinic (398.9 eV), pyrrolic (400.4 eV), graphitic
20 (401.3 eV) and oxidized (403.8 eV) nitrogen species, respectively.[46] Pyridinic N was found to be the prominent species at 600 °C together with a few pyrrolic N and less graphitic N. As the temperature increases, the unstable pyrrolic nitrogen atom gradually turns to graphitic nitrogen atom,[45] which has been
25 proposed to promote four-electron process in ORR.[8] For the sample prepared at 900 °C, although it contains a high content of graphitic N, the overall nitrogen content is quite low and the pyridinic N is significantly reduced. Thus the ORR catalitic activity is quite low for the sample activated at 900 °C.
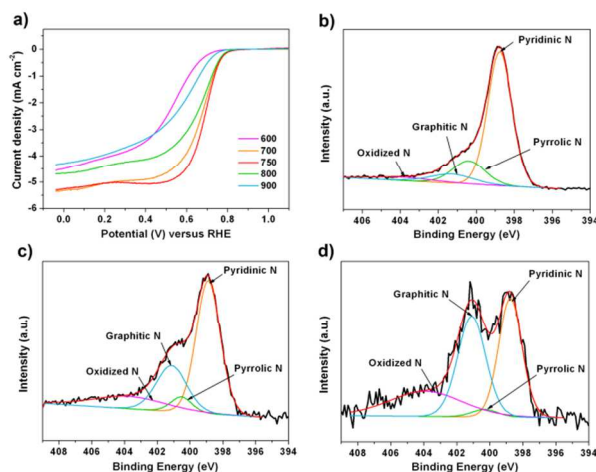
30 **Fig. 5** (a) RDE polarization curves of 300 nm MDC prepared at various temperatures. (b-d) N 1s XPS spectra of MDC prepared at 600 °C (b), 750 °C (c) and 900 °C (d).

There are two important features rendering nano MDC with
35 superior ORR activity. Firstly, the usage of MOF ensures the abundant Co-N$_4$ moieties which would be further converted to active site and the high surface area in the derived catalyst. Compared to the previous best performed catalyst precursors,[12,13] mixtures of carbon supports, nitrogen precursors and transition-
40 metal salts, MOF has the nature of molecular defined 3D-structure, which means not only the abundant desired moieties but also the uniform distribution of such sites. Moreover, the porous character of the MOF is handed down to MDC. Therefore

an open catalytic system with abundant and uniform active site
45 was achieved through the MOF precursors. Secondly, the small size of the nano catalyst improves the mass-transport property. Oxygen reduction reaction involves a triple-phase system, the solid catalyst, the liquid electrolyte and the oxygen gas. So efficient transport of O$_2$, protons and H$_2$O these ORR-related
50 species in the triple-phase boundary is beneficial. Here, our catalyst has the ideal structure for this purpose. The catalytic sites are uniformly distributed on the fully exposed walls of the carbon polyhedron, which accelerates mass exchange rate, hence further improving the ORR activity.

Conclusions

We have for the first time employed nano MOFs to fabricate promising ORR electrocatalyst. Size effects of the MOF precursor on the catalytic properties are systematically revealed in this work. As the particle size decreases, the catalytic activity
60 increases markedly. The best electrocatalysts evolved from the smallest MOF precursor (300nm) exhibits novel activity and superior stability in acidic solution. The high activity of the nano-electrocatalyst is attributed to the fully exposed nanostructure with good mass- and electron-transport properties. The present
65 work demonstrates that small MOFs can impressively make a big difference, which opens new avenues for the flourishing application of MOFs.

Acknowledgements

75 Notes and references

Beijing Key Lab of Advanced Battery Materials, Department of Materials Science and Engineering, College of Engineering, Peking University, Beijing 100871, P. R. China.
E-mail: rzou@pku.edu.cn
80 † Electronic Supplementary Information (ESI) available: [Supplementary Figs. S1-S35 and Table S1,2]. See DOI: 10.1039/b000000x/

1 B. C. H. Steele and A. Heinzel, *Nature*, 2001, **414**, 345.
2 H. A. Gasteiger and N. M. Marković, *Science*, 2009, **324**, 48.
3 H. A. Gasteiger, S. S. Kocha, B. Sompalli and F. T. Wagner, *Appl.*
85 *Catal. B: Environ.*, 2005, **56**, 9.
4 J. B. Wu and H. Yang, *Acc. Chem. Res.*, 2013, **46**, 1848.
5 D. J. Berger, *Science*, 1999, **286**, 49.
6 F. Jaouen, E. Proietti, M. Lefèvre, R. Chenitz, J. P. Dodelet, G. Wu, H. T. Chung, C. M. Johnston and P. Zelenay, *Energy Environ. Sci.*,
90 2011, **4**, 114.
7 G. Wu and P. Zelenay, *Acc. Chem. Res.*, 2013, **46**, 1878.
8 R. Silva, D. Voiry, M. Chhowalla and T. Asefa, *J. Am. Chem. Soc.*, 2013, **135**, 7823.
9 K. P. Gong, F. Du, Z. H. Xia, M. Durstock and L. M. Dai, *Science*,
95 2009, **323**, 760.
10 Y. Y. Liang, Y. G. Li, H. L. Wang, J. G. Zhou, J. Wang, T. Regier and H. J. Dai, *Nat. Mater.*, 2011, **10**, 780.
11 Y. G. Li, W. Zhou, H. L. Wang, L. M. Xie, Y. Y. Liang, F. Wei, J-C. Idrobo, S. J. Pennycook and H. J. Dai, *Nat. Nanotechnol.*, 2012, **7**,
100 394.

12 G. Wu, K. L. More, C. M. Johnston and P. Zelenay, *Science*, 2011, **332**, 443.

13. M. Lefèvre, E. Proietti, F. Jaouen and J-P. Dodelet, *Science*, 2009, **324**, 71.

14. S. L. James, *Chem. Roc. Rev.*, 2003, **32**, 276.

15. J. L. C. Rowsell and O. M. Yaghi, *Microporous Mesoporous Mater.*, 2004, **73**, 3.

16 N. W. Ockwig, O. Delgado-Friedrichs, M. O'Keeffe and O. M. Yaghi, *Acc. Chem. Res.*, 2005, **38**, 176.

17 J. R. Li, R. J. Kuppler and H. C. Zhou, *Chem. Soc. Rev.*, 2009, **38**, 1477.

18 D. Farrusseng, S. Aguado and C. Pinel, *Angew. Chem. Int. Ed.*, 2009, **48**, 7502.

19 M. Kurmoo, *Chem. Soc. Rev.*, 2009, **38**, 1353.

20 M. D. Allendorf, C. A. Bauer, R. K. Bhakta and R. J. T. Houk, *Chem. Soc. Rev.*, 2009, **38**, 1330.

21 S. L. Li and Q. Xu, *Energy Environ. Sci.*, 2013, **6**, 1656.

22 B. Liu, H. Shioyama, T. Akita and Q. Xu, *J. Am. Chem. Soc.*, 2008, **130**, 5390.

23 H. L. Jiang, B. Liu, Y. Q. Lan, K. Kuratani, T. Akita, H. Shioyama, F. Q. Zong and Q. Xu, *J. Am. Chem. Soc.*, 2011, **133**, 11854.

24 M. Hu, J. Reboul, S. Furukawa, N. L. Torad, Q. M. Ji, P. Srinivasu, K. Ariga, S. Kitagawa and Y. Yamauchi, *J. Am. Chem. Soc.*, 2012, **134**, 2864.

25 W. Xia, B. Qiu, D. G. Xia and R. Q. Zou, *Sci. Rep.*, 2013, **3**, 1935.

26 Q. F. Wang, W. Xia, W. H. Guo, L. An. D. G. Xia and R. Q. Zou, *Chem. Asian J.*, 2013, **8**, 1879.

27 L. Zhang, H. B. Wu, S. Madhavi, H. H. Hng and X. W. Lou, *J. Am. Chem. Soc.*, 2012, **134**, 17388.

28 X. D. Xu, R. G. Cao, S. Jeong and J. Cho, *Nano Lett.*, 2012, **12**, 4988.

29 S. J. Yang, S. Nam, T. Kim, J. H. Im, H. Jung, J. H. Kang, S. Wi, B. Park and C. R. Park, *J. Am. Chem. Soc.*, 2013, **135**, 7394.

30 T. K. Kim, K. J. Lee, J. Y. Cheon, J. H. Lee, S. H. Joo and H. R. Moon, *J. Am. Chem. Soc.*, 2013, **135**, 8940.

31 S. Q. Ma, G. A. Goenaga, A. V. Call and D. J. Liu, *Chem. Eur. J.*, 2011, **17**, 2063.

32 D. Zhao, J. L. Shui, C. Chen, X. Q. Chen, B. M. Reprogle, D. P. Wang and D. J. Liu, *Chem. Sci.*, 2012, **3**, 3200.

33 E. Proietti, F. Jaouen, M. Lefèvre, N. Larouche, J. Tian, J. Herranz and J. P. Dodelet, *Nat. Commun.*, 2011, **2**, 416.

34 J. Tian, A. Morozan, M. T. Sougrati, M. Lefèvre, R. Chenitz, J. P. Dodelet, D. Jones and F. Jaouen, *Angew. Chem. Int. Ed.*, 2013, **52**, 1.

35 K. S. Park, Z. Ni, A. P. Côté, J. Y. Choi, R. D. Huang, F. J. Uribe-Romo, H. K. Chae, M. O'Keeffe and O. M. Yaghi, *Proc. Natl. Acad. Sci. USA.*, 2006, **103**, 10186.

36 R. Banerjee, A. Phan, B. Wang, C. Knobler, H. Furukawa, M. O'Keeffe and O. M. Yaghi, *Science*, 2008, **319**, 939.

37 S. K. Nune, P. K. Thallapally, A. Dohnalkova, C. M. Wang, J. Liu and G. J. Exarhos, *Chem. Commun.*, 2010, **46**, 4878.

38 J. Cravillon, R. Nayuk, S. Springer, A. Feldhoff, K. Huber and M. Wiebcke, *Chem. Mater.*, 2011, **23**, 2130.

39 Z. Ni and R. I. Masel, *J. Am. Chem. Soc.*, 2006, **128**, 12394.

40 B. Seoane, J. M. Zamaro, C. Tellez and J. Coronas, *CrystEngComm*, 2012, **14**, 3103.

41 F. Jaouen, J. Herranz, M. Lefèvre, J. P. Dodelet, U. I. Kramm, I. Herrmann, P. Bogdanoff, J. Maruyama, T. Nagaoka, A. Garsuch, J. R. Dahn, T. Olson, S. Pylypenko, P. Atanassov and E. A. Ustinov, *ACS Appl. Mater. Interfaces*, 2009, **1**, 1623.

42 A. A. Gewirth and M. S. Thorum, *Inorg. Chem.*, 2010, **49**, 3557.

43 A. Bonakdarpour, M. Lefèvre, R. Z. Yang, F. Jaouen, T. Dahn, J. P. Dodelet and J. R. Dahn, *Electrochem. Solid-State Lett.*, 2008, **11**, B105.

44 C. W. B. Bezerra, L. Zhang, K. C. Lee, H. S. Liu, A. L. B. Marques, E. P. Marques, H. J. Wang and J. J. Zhang, *Electrochim. Acta*, 2008, **53**, 4937.

45 G. Wu, N. H. Mack, W. Gao, S. G. Ma, R. Q. Zhong, J. T. Han, J. K. Baldwin and P. Zelenay, *ACS Nano*, 2012, **6**, 9764.

46 J. R. Pels, F. Kapteijn, J. A. Moulijn, Q. Zhu and K. M. Thomas, *Carbon*, 1995, **33**, 1641.

Table of Contents
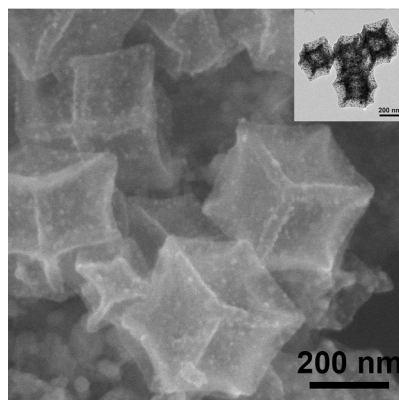
Well-defined porous carbon polyhedrons are synthesized directly from MOF nanocrystals and shows

5 high ORR catalytic activity in acid media.